

Observation of $B \rightarrow D^* \pi^+ \pi^- \pi^- \pi^0$ Decays

Abstract

We report on the observation of $B \rightarrow D^* \pi^+ \pi^- \pi^- \pi^0$ decays. The branching ratio's for D^{*+} and D^{*0} are $(1.72 \pm 0.14 \pm 0.24)\%$ and $(1.80 \pm 0.24 \pm 0.25)\%$, respectively. Approximately 20% of each final state has a $D^* \omega \pi^-$ component. The $\omega \pi^-$ appears to come from the decay of a resonance of mass 1419 ± 33 MeV and width 382 ± 44 MeV, that has spin > 0 .

1 Introduction

We report an analysis from a data sample consisting of 9.0 fb^{-1} of integrated luminosity taken with the CLEO II and II.V detectors using the CESR e^+e^- storage ring on the peak of the $\Upsilon(4S)$ resonance and 4.4 fb^{-1} in the continuum at 60 MeV less center-of-mass energy. The sample contains 19.4 million B mesons.

Currently, measured exclusive branching ratios for hadronic B decays total a small fraction of the total hadronic width. The total semileptonic branching ratio for $B \rightarrow X e^- \nu$, $X \mu^- \nu$, and $X \tau^- \nu$ totals approximately 25% [1]. The measured hadronic decay modes for the \overline{B}^0 including $D^+(n\pi^-)$, $D^{*+}(n\pi^-)$, where $3 \geq n \geq 1$, $D^{+(*)} D_s^{-(*)}$, and J/ψ exclusive totals only about 10% [1]. (The B^- modes total about 15% more.) It is also interesting to note that the average charged multiplicity in a hadronic B^0 decay is 5.3 ± 0.1 [2]. Since the average multiplicity contains contributions from the D^+ or D^{*+} normally present in \overline{B}^0 decay, we expect a sizeable, approximately several percent, decay rate into final states with four pions [3]. The seen $D^{(*)}(n\pi)^-$ final states for $n \leq 3$ are consistent with being quasi-two-body final states. For n of two the ρ^- dominates, while for n of three the a_1^- dominates [4]. It would be interesting to see if this behavior remains true for n of 4.

2 Observation of $\overline{B}^0 \rightarrow D^{*+} \pi^+ \pi^- \pi^- \pi^0$ Decays

2.1 Event selection

We start by investigating the $D^{*+}(4\pi)^-$ final state. Track candidates are required to pass a series of cuts listed in the appendix. Photon candidates are required to be within the "good barrel region," within 45° of the normal to the beam line. We select events with a D^{*+} using the $\pi^+ D^0$ decay. We use three D^0 final states: $K^- \pi^+$, $K^- \pi^+ \pi^0$, and $K^- \pi^+ \pi^+ \pi^-$.

We require that the invariant mass of the D^0 candidates lie within $\pm 2.5\sigma$ of the known D^0 mass and that the mass difference between $\pi^+ D^0$ and D^0 combinations is within $\pm 2.5\sigma$. The σ 's are listed in Table 1. The D^0 widths vary with the D^0 momentum, p , (units of MeV). We did not find significant differences between the CLEO II and II.V data sets.

Table 1: Mass Resolutions (σ) in MeV

$D^{*+} - D^0$	$D^{*0} - D^0$	$D^0 \rightarrow K^- \pi^+$	$D^0 \rightarrow K^- \pi^+ \pi^0$	$D^0 \rightarrow K^- \pi^+ \pi^+ \pi^-$
0.63	0.90	$p \times 0.93 \times 10^{-3} + 6.0$	$p \times 0.68 \times 10^{-3} + 11.6$	$p \times 0.92 \times 10^{-3} + 4.7$

Neutral pions are formed by selecting photon pairs that are in the good barrel region; they are required to have E9/E25 probabilities greater than 99% and not be fragments (see appendix). The photons pairs then are required to have an invariant mass within -3 and $+2.5 \sigma$ of the π^0 mass.

The D^{*+} candidates are combined with all combinations of $\pi^+ \pi^- \pi^- \pi^0$ mesons. To reject continuum we require that the Fox-Wolfram moment R_2 be less than 0.3 [5].

Next, we calculate the difference between the beam energy, E_{beam} , and the measured energy of the five particles, ΔE . The “beam constrained” invariant mass of the B candidates, M_B , is computed from the formula

$$M_B^2 = E_{beam}^2 - \left(\sum_i \vec{p}_i \right)^2 \quad . \quad (1)$$

To further reduce backgrounds we define

$$\chi_b^2 = \left(\frac{\Delta M_{D^*}}{\sigma(\Delta M_{D^*})} \right)^2 + \left(\frac{\Delta M_D}{\sigma(\Delta M_D)} \right)^2 + \left(\frac{\Delta M_{\pi^0}}{\sigma(\Delta M_{\pi^0})} \right)^2 \quad , \quad (2)$$

where ΔM_{D^*} is the computed $D^* - D^0$ mass difference, ΔM_D is the invariant candidate D^0 mass minus the known D^0 mass and ΔM_{π^0} is the measured $\gamma\gamma$ invariant mass minus the known π^0 mass. All π^0 's in the final state are included in the sum. The σ 's are the measurement errors. We select candidate events in each mode requiring that $\chi_b^2 < C_n$, where C_n varies for each decay D^0 decay mode. For the $Kn\pi$ decay modes we use $C_n = 12$, 8, and 6, respectively. The χ_b^2 spectra for data and Monte Carlo are shown in Fig. 1.

2.2 Branching Fraction and $(4\pi)^-$ Mass Spectrum

We start with the $D^0 \rightarrow K^- \pi^+$ decay mode. We show the candidate B mass distribution, M_B for events with the difference between the measured B energy and the beam energy, ΔE , is not centered on zero but is in the bands from -5.0 to -3.0σ and 5.0 to 3.0σ on Fig. 2(a). The ΔE resolution is 18 MeV (σ). This gives a good representation of the background in the signal region. We fit this distribution with a shape given as

$$back(r) = p_1 r \sqrt{1 - r^2} e^{-p_2(1-r^2)} \quad , \quad (3)$$

where $r = M_B/5.2895$, and the p_i are parameters given by the fit.

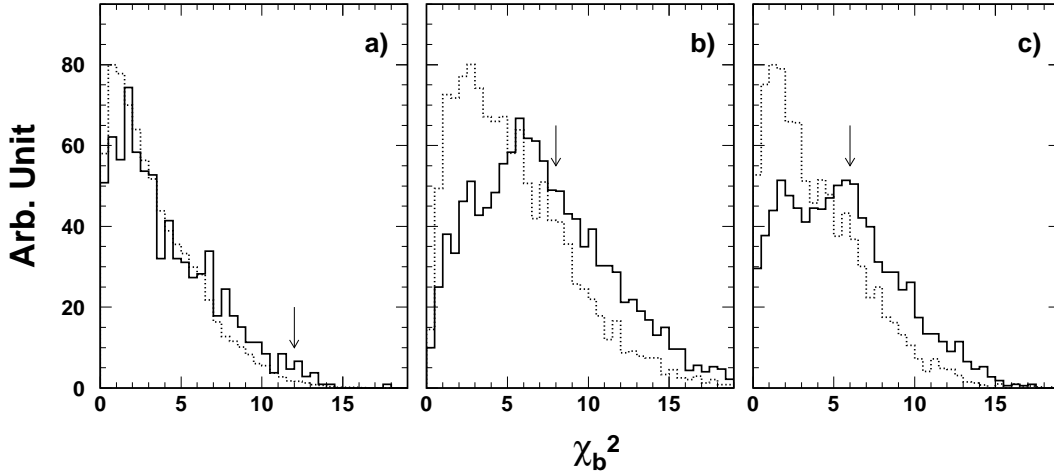


Figure 1: The χ_b^2 spectra for the final state $\overline{B}^0 \rightarrow D^{*+}\pi^+\pi^-\pi^-\pi^0$ for (a) $D^0 \rightarrow K^-\pi^+$, (b) $D^0 \rightarrow K^-\pi^+\pi^0$, and (c) $D^0 \rightarrow K^-\pi^+\pi^+\pi^-$. The solid line is the data, the dashed signal Monte Carlo and the arrows indicate the selected cut values. For the data we restrict ΔE to be within of 2σ zero and an M_B to be within 2σ of the known B^0 mass.

We next view the M_B distribution for events having ΔE within 2σ around zero in Fig. 2(b). This distribution is fit with a Gaussian signal function of width 2.7 MeV and the background function found above whose normalization is allowed to vary. We find 358 ± 29 events in the signal peak.

We repeat this procedure for the other two D^0 decay modes. The M_B spectrum for ΔE sidebands and signal region is shown in Figs. 3 and 4. The ΔE resolution is 22 MeV in the $K^-\pi^+\pi^0$ mode and 18 MeV in the $K^-\pi^+\pi^+\pi^-$ mode. Signals for these two decay modes are weaker than in $K^-\pi^+$ but present. The number of signal events in each mode are shown in Table 2.

Table 2: Event numbers for the $D^{*+}\pi^+\pi^-\pi^-\pi^0$ final state

D^0 Decay Mode	Fitted # of events (%)
$K^-\pi^+$	358 ± 29
$K^-\pi^+\pi^0$	543 ± 49
$K^-\pi^+\pi^+\pi^-$	329 ± 41

We can view the signal by selecting those events in the M_B signal region within 2σ of the B^0 mass, and plotting the ΔE distribution, as shown in Fig. 5. Clear peaks near ΔE of zero are seen.

We choose to determine the branching fraction using only the $D^0 \rightarrow K^-\pi^+$ decay mode because of the relatively large backgrounds in the other modes and the decreased systematic error due to having fewer particles in the final state. In order to find the branching ratio we use the Monte Carlo generated efficiency, shown in Fig. 6 as a function of $(4\pi)^-$ mass.

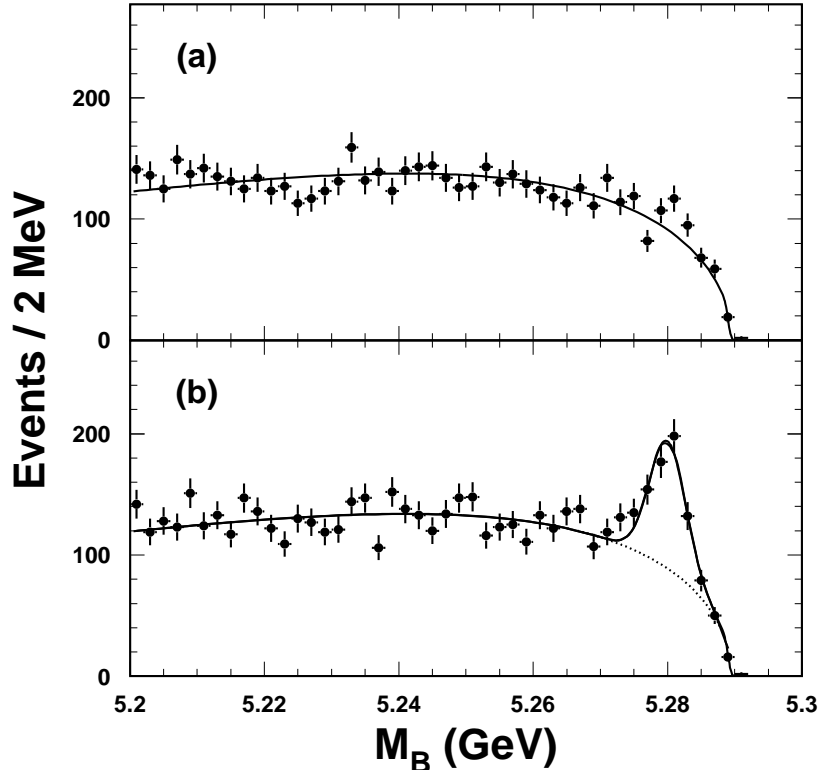


Figure 2: The B candidate mass spectra for the final state $D^{*+}\pi^+\pi^-\pi^-\pi^0$, with $D^0 \rightarrow K^-\pi^+$ (a) for ΔE sidebands and (b) for ΔE consistent with zero. The curve in (a) is a fit to the background distribution described in the text, while in (b) the shape from (a) is used with the normalization allowed to float and a signal Gaussian of width 2.7 MeV is added.

The efficiency falls off at larger $(4\pi)^-$ masses because the detection of the slow π^+ from the D^{*+} decay becomes increasingly difficult. Since the efficiency varies with mass we need to determine the $(4\pi)^-$ mass spectrum. To rid ourselves of the problem of the background shape, we fit the B candidate mass spectrum in 50 MeV bins of 4π mass. (The mass resolution is approximately 12 MeV.) The resulting $(4\pi)^-$ mass spectrum is shown in Fig. 7. There may be a low mass structure around 1.5 GeV. This will be investigated further in this paper.

We find

$$\mathcal{B}(\overline{B}^0 \rightarrow D^{*+}\pi^+\pi^+\pi^-\pi^0) = (1.72 \pm 0.14 \pm 0.24)\% \quad . \quad (4)$$

The systematic error arises mainly from our lack of knowledge about the tracking and π^0 efficiencies. We assign errors of $\pm 2.2\%$ on the efficiency of each charged track, $\pm 5\%$ for the slow pion from the D^{*+} , and $\pm 5.4\%$ for the π^0 [6]. The error due to the background shape is evaluated in three ways. First of all, we change the background shape by varying the fitted parameters by 1σ . This results in a change of $\pm 3\%$. Secondly, we allow the shape, p_2 , to vary (the normalization, p_1 , was already allowed to vary). This results in 3.8% increase in

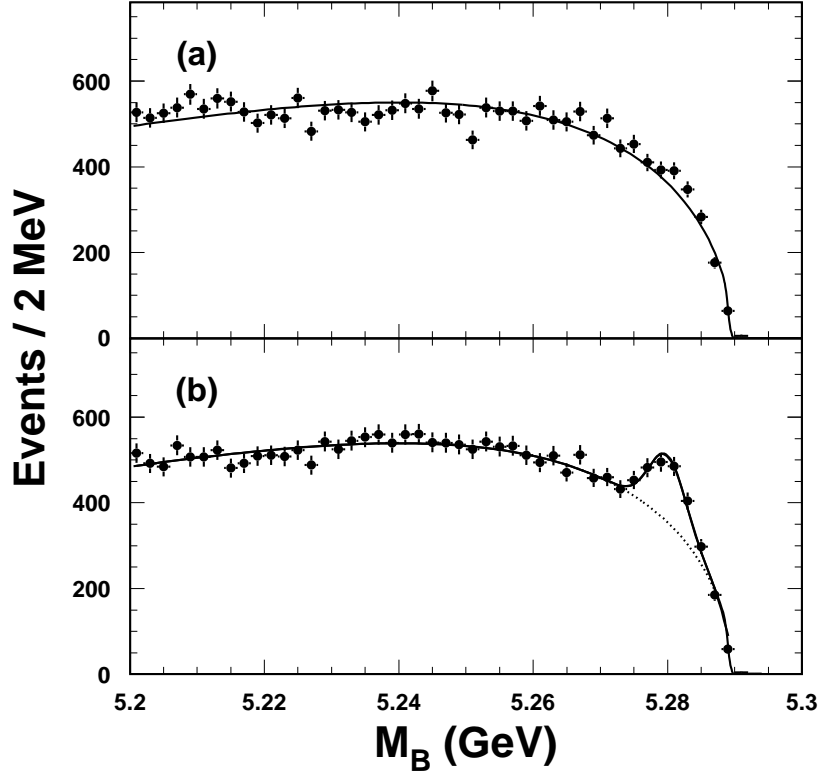


Figure 3: The B candidate mass spectra for the final state $D^{*+}\pi^+\pi^-\pi^-\pi^0$, with $D^0 \rightarrow K^-\pi^+\pi^0$ (a) for ΔE sidebands and (b) for ΔE consistent with zero. The curve in (a) is a fit to the background distribution described in the text, while in (b) the shape from (a) is used with the normalization allowed to float and a signal Gaussian of width 2.7 MeV is added.

the number of events. Finally, we choose a different background function

$$back'(r) = p_1 r \sqrt{1 - r^2} (1 + p_2 r + p_3 r^2 + p_4 r^3) \quad , \quad (5)$$

and repeat the fitting procedure. This results in a 3.7% decrease in the number of events. Taking a conservative estimate of the systematic error due to the background shape we arrive at $\pm 3.8\%$. We use the current particle data group values for the relevant D^{*+} and D^0 branching ratios of $(68.3 \pm 1.4)\%$ ($D^{*+} \rightarrow \pi^+ D^0$) and $(3.85 \pm 0.09)\%$ ($D^0 \rightarrow K^-\pi^+$), respectively [1]. The relative errors, 2.0% for the D^{*+} branching ratio and 2.3% for the D^0 are added in quadrature to the other sources of systematic error, yielding a total systematic error of 10%.

We wish to search for narrow structures. However, we cannot fit the B mass spectrum in small $(4\pi)^-$ mass intervals due to a lack of statistics. Thus we plot the $(4\pi)^-$ mass for events in the M_B peak for the $D^0 \rightarrow K^-\pi^+$ mode and the sum of all three modes in Fig. 8. We also plot two background samples: events at lower M_B (5.203 - 5.257 GeV) and those in the ΔE sideband separately.

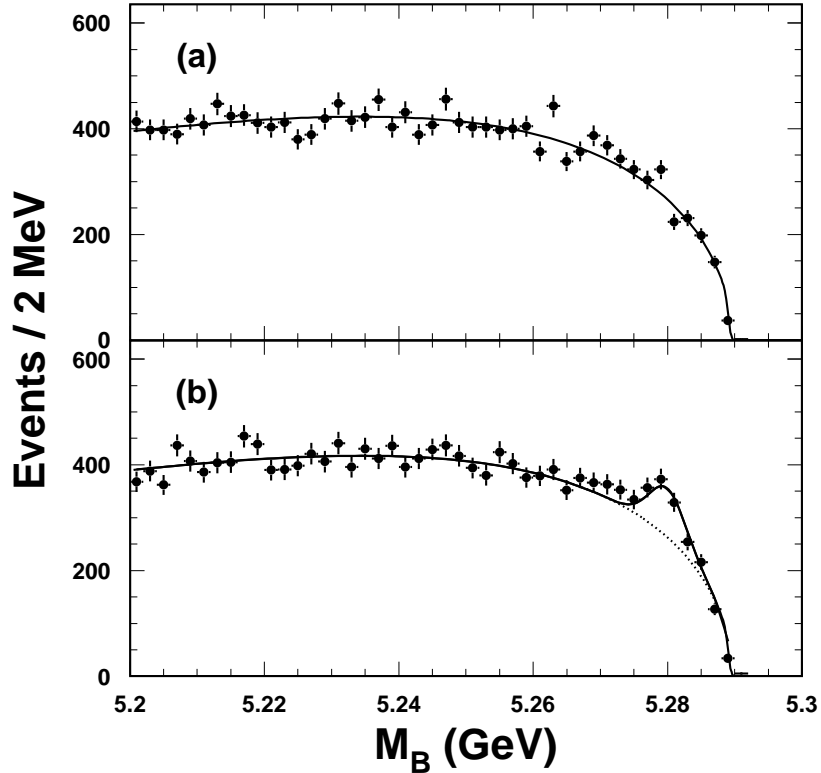


Figure 4: The B candidate mass spectra for the final state $D^{*+}\pi^+\pi^-\pi^-\pi^0$, with $D^0 \rightarrow K^-\pi^+\pi^+\pi^-$ (a) for ΔE sidebands and (b) for ΔE consistent with zero. The curve in (a) is a fit to the background distribution described in the text, while in (b) the shape from (a) is used with the normalization allowed to float and a signal Gaussian of width 2.7 MeV is added.

First we view the plots in the canonical 50 MeV bins. Both background distributions give a consistent if somewhat different estimates of the background shape. (Each background distribution has been normalized to the absolute number of background events as determined by the fit to the M_B distribution.) In any case no prominent narrow structures appear in the histograms for the 10 MeV binning.

3 The $\bar{B}^0 \rightarrow D^{*+}\omega\pi^-$ Reaction

To investigate the composition of the $(4\pi)^-$ final state, we now investigate the $\pi^+\pi^-\pi^0$ mass spectrum for the events in the B peak. All three D^0 decay modes are used. We show the $\pi^+\pi^-\pi^0$ invariant mass distribution for events in the B mass peak in Fig. 9 (there are two combinations per event). A clear signal is visible at the ω . The histogram on the figure is for events in the lower M_B range, from 5.203 GeV to 5.257 GeV. No ω signal is visible here.

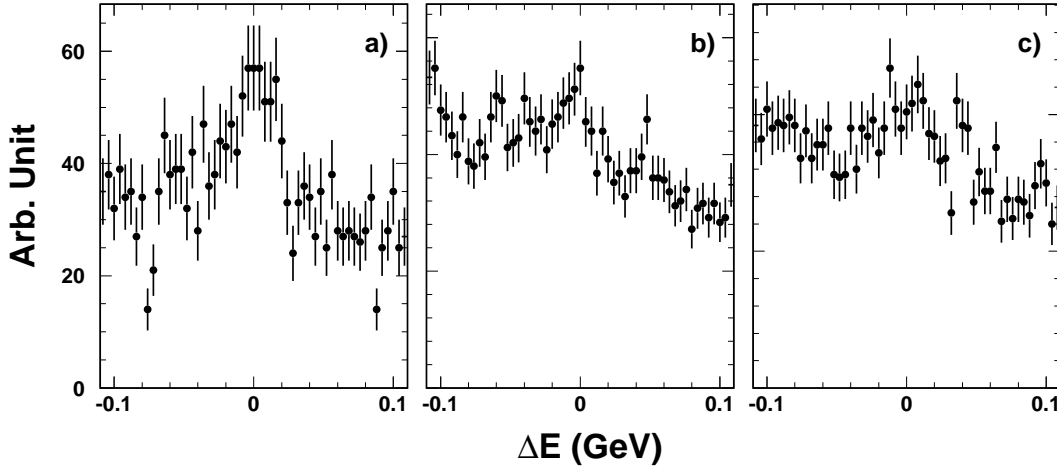


Figure 5: The ΔE spectrum for the final state $D^{*+}\pi^+\pi^-\pi^-\pi^0$ restricted to combinations within 2σ of the B^0 mass with (a) $D^0 \rightarrow K^-\pi^+$ (b) $D^0 \rightarrow K^-\pi^+\pi^0$, and (c) $D^0 \rightarrow K^-\pi^+\pi^+\pi^-$.

The purity of the ω sample can be further improved by examining the Dalitz plot of the decay products. We define a cut on the Dalitz plot as follows. Let T_0 , T_+ and T_- be the kinetic energies of the pions and Q be the difference between the ω mass, M_ω and the mass of the 3 pions. We define two orthogonal coordinates X and Y , where

$$X = 3T_0/Q - 1 \quad (6)$$

$$Y = \sqrt{3}(T_+ - T_-)/Q \quad (7)$$

The kinematic limit that defines the Dalitz plot boundary is defined as

$$Y_{boundary}^2 = \frac{1}{3}(X_{boundary} + 1)(X_{boundary} + 1 + a)(1 + b/(X_{boundary} + 1 - c)) \quad (8)$$

where $a = 6m_0/Q$, $b = 6m^2/(M_\omega Q)$, $c = 3(M_\omega - m_0)^2/(2M_\omega Q)$, m is the mass of a charged pion and m_0 the mass of the neutral pion.

For any set of three pion kinetic energies, we define a variable r , properly scaled to the kinematic limit as

$$r = \sqrt{\frac{X^2 + Y^2}{X_{boundary}^2 + Y_{boundary}^2}} \quad (9)$$

where the boundary values are found by following the radial vector from $(0,0)$ through (X, Y) .

For events in the B mass peak we show in Fig. 10 the $\pi^+\pi^-\pi^0$ invariant mass for three different cuts on r . The ω signal is purified by using a selection on r .

For further analysis we select ω candidates within the the $\pi^+\pi^-\pi^0$ mass window of 782 ± 20 MeV with $r < 0.7$. We also abandon the χ^2 cut as background is less of a problem. In Fig. 11 we show the B candidate mass distribution for the $D^{*+}\omega\pi^-$ final state summing over all three D^0 decay modes. (The signal is fit with the same prescription as before.)

In Fig. 12 we show the $\omega^0\pi^-$ mass spectrum in the left-side plot. The solid histogram shows events from the lower M_B sideband region suitably normalized. The dotted histogram

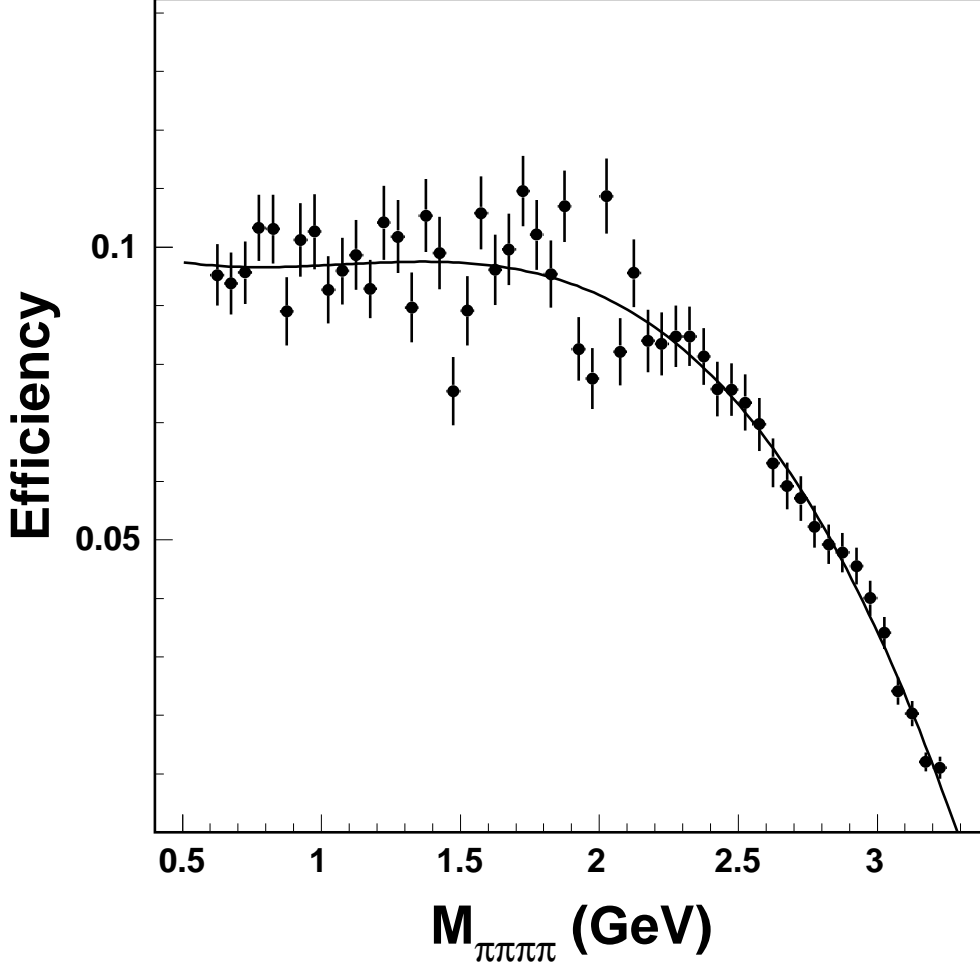


Figure 6: The efficiency for the final state $D^{*+}\pi^+\pi^-\pi^-\pi^0$, with $D^0 \rightarrow K^-\pi^+$.

shows the background estimate from the ΔE sidebands, again normalized. In the signal distribution there is a wide structure around 1.4 GeV, that is inconsistent with background. We redetermine the $\omega\pi^-$ mass distribution by fitting the M_B distribution in bins of $\omega\pi^-$ mass, and this is shown on the right-side. Fitting to a Breit-Wigner function, we find a peak value of 1416 ± 37 MeV and a width of 402 ± 47 MeV. These numbers change to 1432 ± 37 MeV and 376 ± 47 MeV, respectively, after applying a correction for the variation of efficiency with mass. The systematic errors are found by varying the background shape and are negligible compared to the statistical error.

Knowing the $\omega\pi^-$ mass dependence we can evaluate the branching fraction:

$$\mathcal{B}(\overline{B}^0 \rightarrow D^{*+}\omega\pi^-) = (0.29 \pm 0.03 \pm 0.04)\% \quad . \quad (10)$$

We tentatively label the state at 1419 MeV the A^- and investigate its properties later. The $\omega\pi^-$ comprises about 17% of the $(4\pi)^-$ final state. All of the $\omega\pi^-$ final state is consistent with coming from A^- decay.

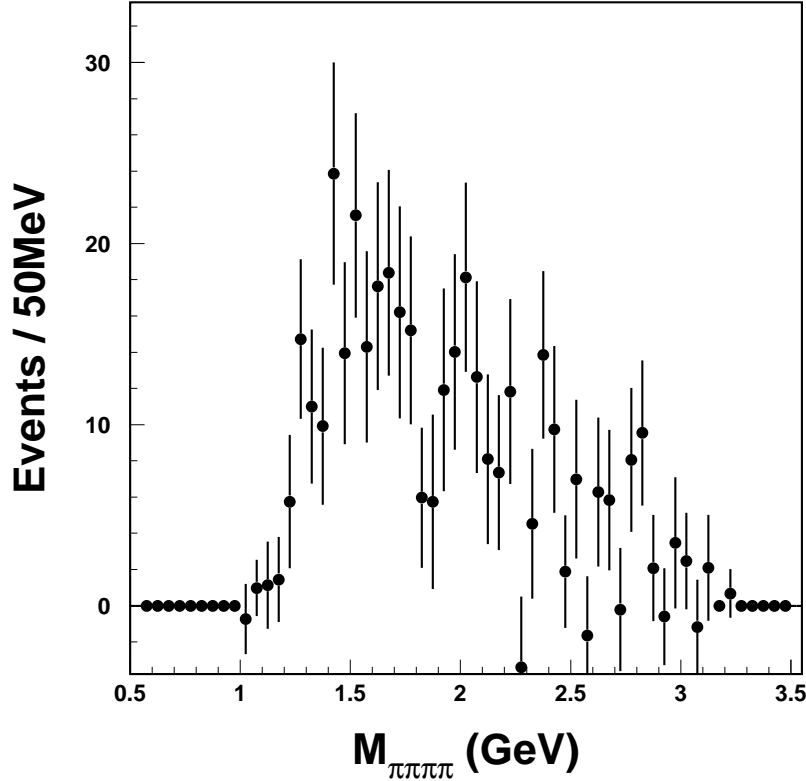


Figure 7: The invariant mass spectra of $\pi^+\pi^-\pi^-\pi^0$ for the final state $D^{*+}\pi^+\pi^-\pi^-\pi^0$, with $D^0 \rightarrow K^-\pi^+$, found by fitting the B yield in bins of 4π mass.

4 Observation of $B^- \rightarrow D^{*0}\pi^+\pi^-\pi^-\pi^0$

We proceed in the same manner as for the \bar{B}^0 reaction with the exception that we use the $D^{*0} \rightarrow \pi^0 D^0$ decay mode and restrict ourselves to the $D^0 \rightarrow K^-\pi^+$ decay mode only due to large backgrounds in the other modes. The χ^2 is calculated according to equation 2 and we use a cut value of 8. The M_B distribution for ΔE sidebands and signal data is shown in Fig. 13 for the $D^0 \rightarrow K^-\pi^+$ decay mode. We see a signal of 195 ± 26 events yielding a branching fraction of

$$\mathcal{B}(B^- \rightarrow D^{*0}\pi^+\pi^-\pi^-\pi^0) = (1.80 \pm 0.24 \pm 0.25)\% \quad . \quad (11)$$

The χ_b^2 and ΔE distributions are shown in Fig. 14.

The $\pi^+\pi^-\pi^0$ mass spectrum shown in Fig. 15 shows the presence of an ω .

Selecting on the presence of an ω with $r < 0.7$ we show the sideband and signal plots in Fig. 16. (Here we do not use the previously defined χ^2 cut.) The branching ratio is

$$\mathcal{B}(B^- \rightarrow D^{*0}\omega\pi^-) = (0.45 \pm 0.10 \pm 0.07)\% \quad . \quad (12)$$

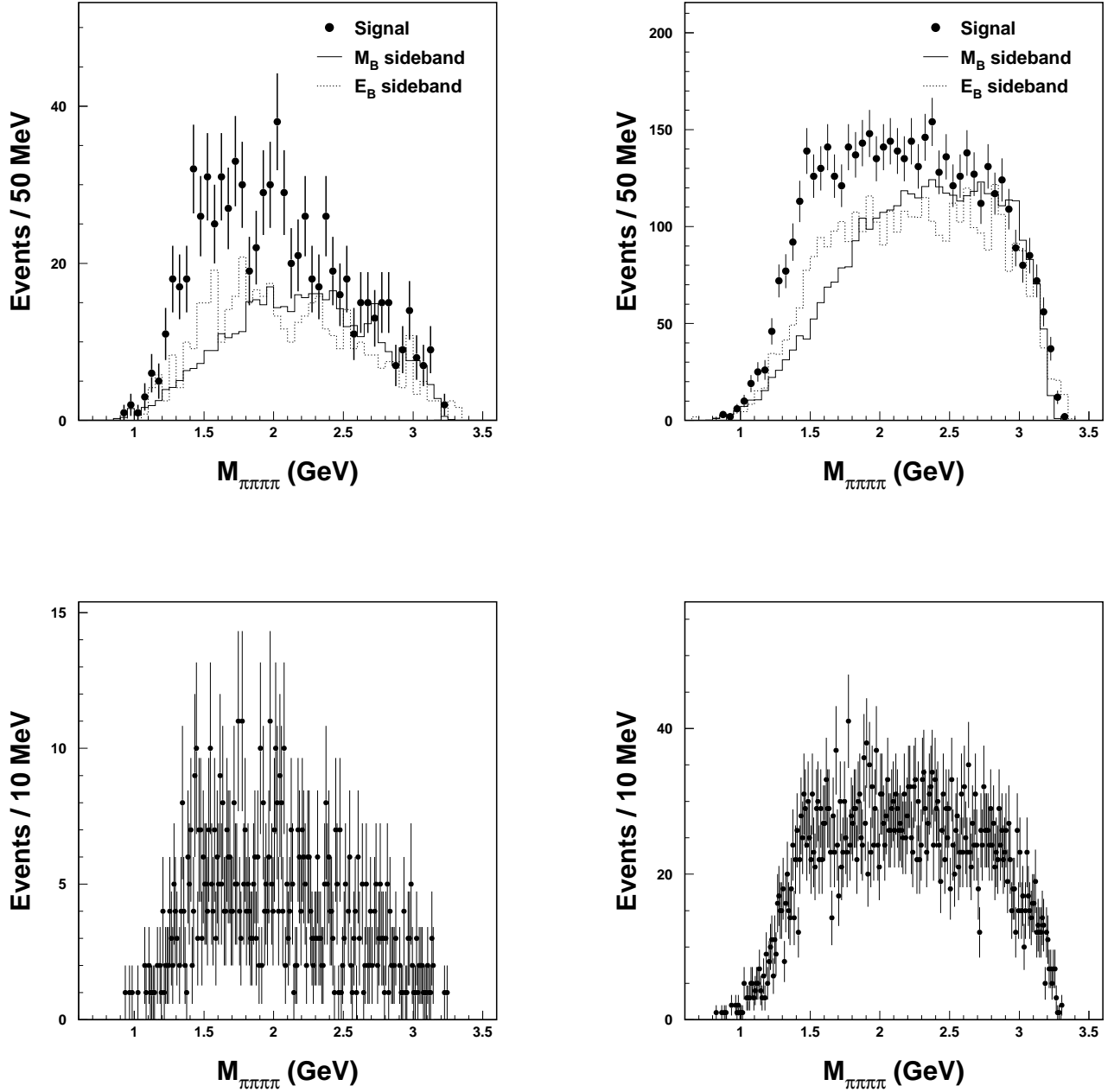


Figure 8: The invariant mass spectra of $\pi^+\pi^-\pi^-\pi^0$ for the final state $D^{*+}\pi^+\pi^-\pi^-\pi^0$, with $D^0 \rightarrow K^-\pi^+$ (upper left), and the sum of all three D^0 decay modes (upper right). Events are selected by being within 2σ of the B mass. The solid histogram is the background estimate from the M_B lower sideband and the dashed histogram is from the ΔE sidebands; both are normalized to the fitted number of background events. The same distributions in smaller bins (lower plots).

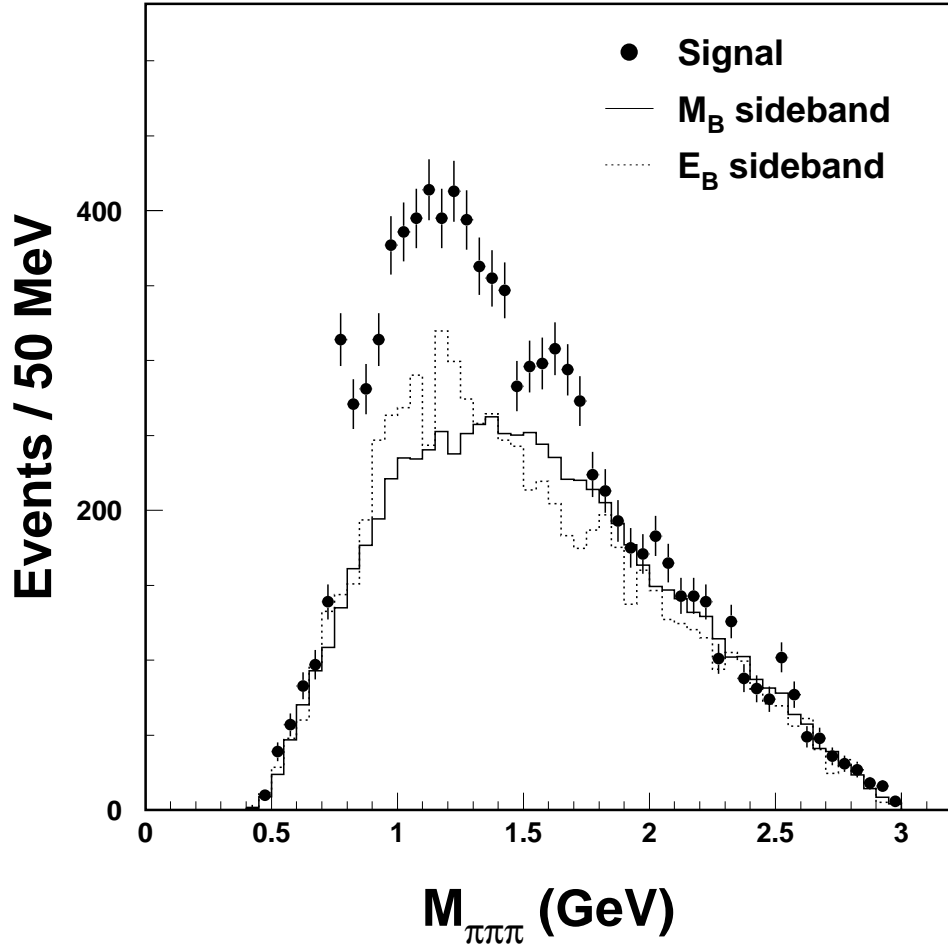


Figure 9: The invariant mass spectra of $\pi^+\pi^-\pi^0$ for the final state $D^{*+}\pi^+\pi^-\pi^-\pi^0$ for all three D^0 decay modes. The solid histogram is the background estimate from the M_B lower sideband and the dashed histogram is from the ΔE sidebands; both are normalized to the fitted number of background events.

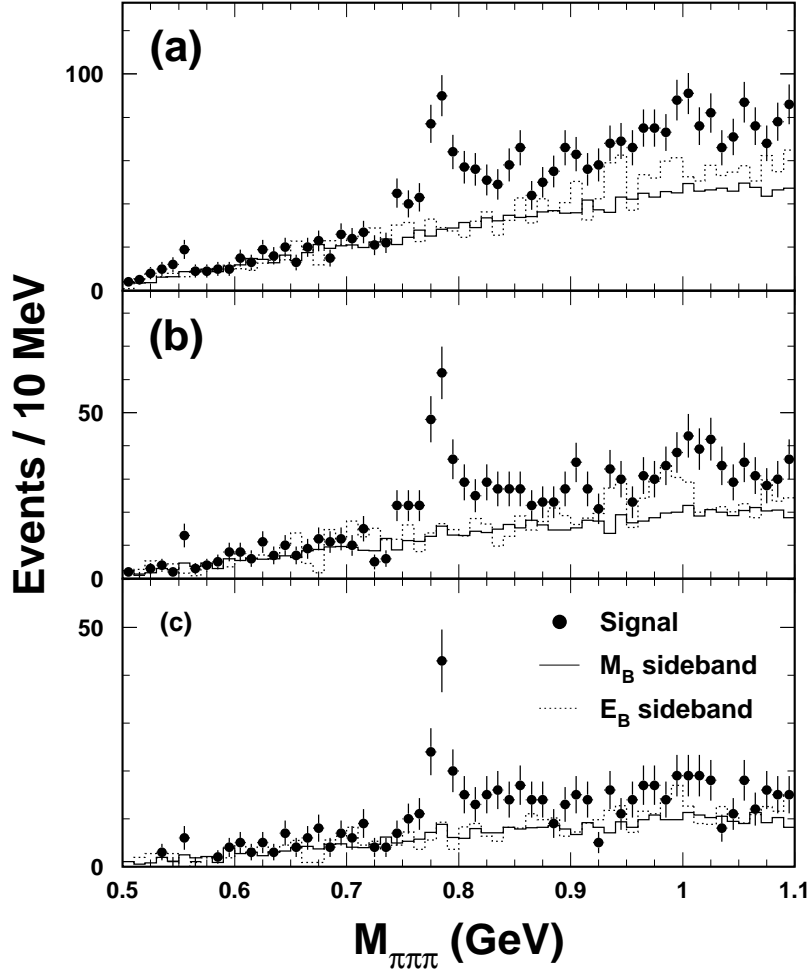


Figure 10: The invariant mass spectra of $\pi^+\pi^-\pi^0$ for the final state $D^{*+}\pi^+\pi^-\pi^-\pi^0$ for all three D^0 decay modes for three selections on r : (a) 1, (b) 0.7 and (c) 0.5. The solid histogram is the background estimate from the M_B lower sideband and the dashed histogram is from the ΔE sidebands; both are normalized to the fitted number of background events.

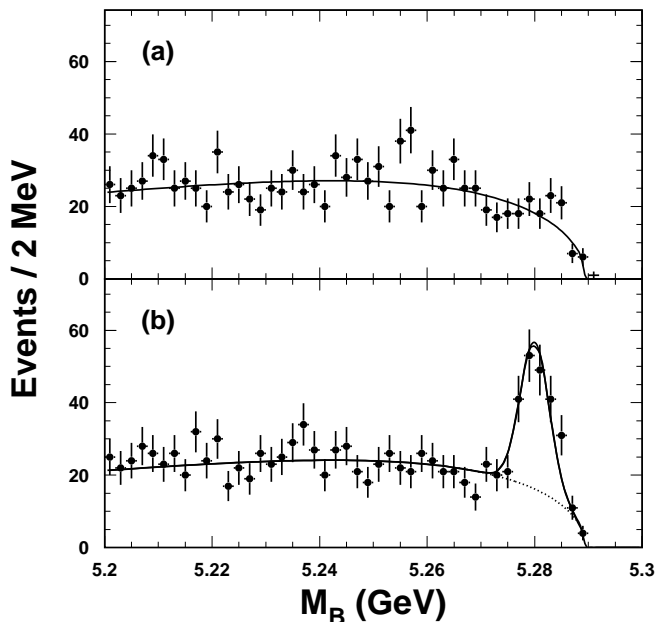


Figure 11: The M_B spectra for $D^{*+}\omega\pi^-$ for all three D^0 decay modes. (a) ΔE sidebands and (b) ΔE around zero.

Similar to the other case the $\omega\pi^-$ fraction of the $(4\pi)^-$ final state is 25%, and all the $\omega\pi^-$ is consistent with coming from the A^- .

In Fig. 17 we show the $\omega\pi^-$ mass spectrum. We see an enhancement at around 1.4 GeV as in the neutral B case. A fit to the data gives a mass of 1367 ± 75 MeV and width of 439 ± 135 MeV, consistent within the large errors with the \bar{B}^0 case. (We do not have enough statistics here to fit the M_B distribution in bins of $\omega\pi^-$ mass.)

For analysis of the angular distributions we add the data from both $D^{*+}\omega\pi^-$ and $D^{*0}\omega\pi^-$ final states.

5 Analysis of Decay Angular Distributions

The A^- is produced along with a spin-1 D^* from a spin-0 B . If the A^- is spin-0 the D^* would be fully polarized in the $(J, J_z) = (1, 0)$ state. If the A^- were to be spin-1 any combinations of z-components would be allowed. It is natural then to examine the helicity angle of the D^{*+} by viewing the cosine of the helicity angle of the π^+ with respect to the B in the D^{*+} rest frame.

Another decay angle that can be examined is that of the $\omega\pi$ system. If the A^- is spin-0, the ω is polarized in the $(1,0)$ state and may be if the A^- is spin-1. Here the helicity angle is defined as the angle between the normal to the ω decay plane and the direction of the A^- in the ω rest frame. For a spin-0 A^- the distribution will be cosine-squared. Again full polarization is possible if the A^- is other than spin-0, but any distribution other than cosine-squared would demonstrate that the spin is not equal to zero.

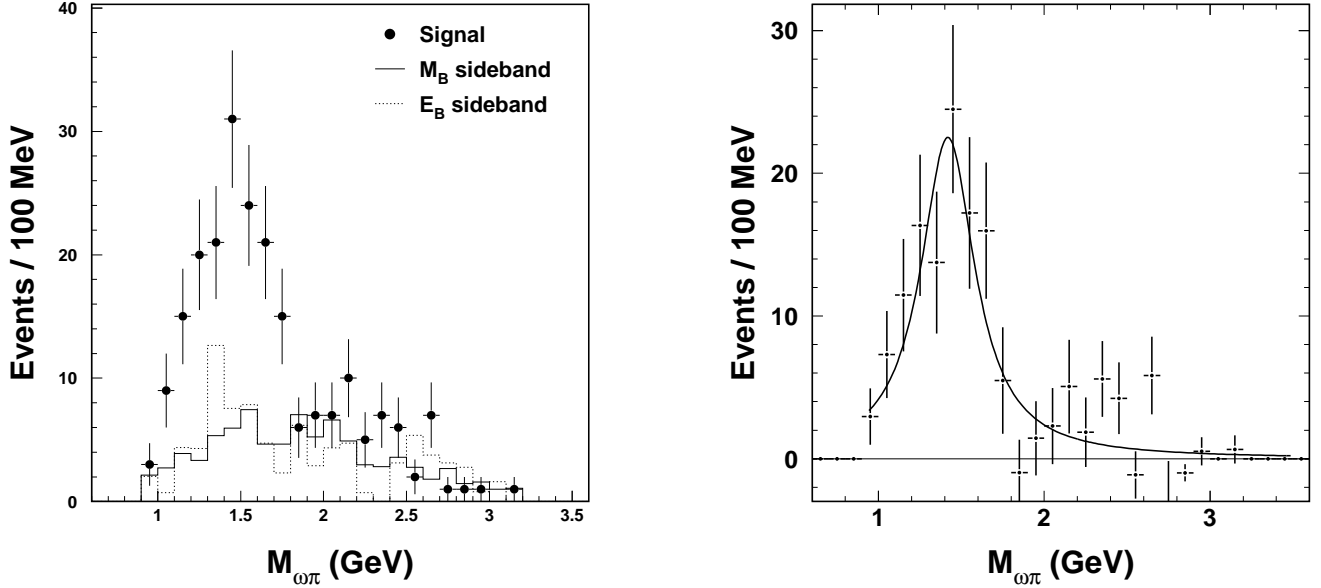


Figure 12: The invariant mass spectra of $\omega\pi^-$ for the final state $D^{*+}\pi^+\pi^-\pi^-\pi^0$ for all three D^0 decay modes. (left) The solid histogram is the background estimate from the M_B lower sideband and the dashed histogram is from the ΔE sidebands; both are normalized to the fitted number of background events. (right) The mass spectrum determined from fitting the M_B distribution and fit to a Breit-Wigner function.

For this analysis we use all three D^0 final states for the D^{*+} final state and the $K^-\pi^+$ final state for the D^{*0} final state, all summed together. To find the distributions we fit the number of events in the M_B candidate plot selected on different angle bins. The $\omega\pi$ mass is required to be between 1.1 and 1.9 GeV.

In Fig. 18 we show the helicity angle distribution, $\cos\theta_{D^*}$ for the D^* decay. We also show the expectations including detector acceptance for spin-0 from the Monte Carlo. The expectation is not symmetric about the zero because the efficiency for very low momentum charged pions goes to zero for slow π^+ . The helicity angle distribution for the $A^- \rightarrow \omega\pi^-$, $\cos\theta_\omega$, is shown on Fig. 19. We have fit the Monte Carlo distributions to the data. The $\cos\theta_{D^*}$ distribution is not consistent with full polarization, yielding a χ^2 of 15 for 4 degrees of freedom. Furthermore the $\cos\theta_\omega$ distribution is quite inconsistent with a $\cos^2\theta_\omega$, yielding a χ^2 of 51 for 4 degrees of freedom.

Therefore, we rule out a spin-0 assignment for the A^- .

6 Search For Other Resonant Substructure

We have accounted for $\sim 20\%$ of the $(4\pi)^-$ final state. We would like to see if there is any further resonant substructure we can disentangle with our current data sample. Since the background is large in modes other than $D^0 \rightarrow K^-\pi^+$ we will only use this mode.

One process that comes to mind is that where the virtual W^- materializes as an a_1^- , that

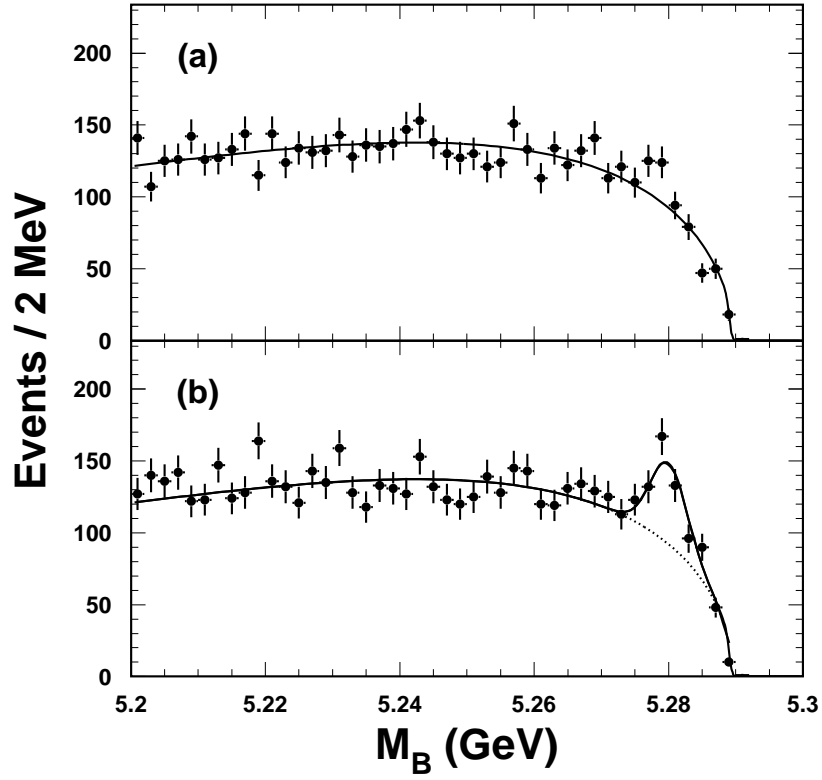


Figure 13: The B candidate mass spectra for the final state $D^{*0}\pi^+\pi^-\pi^-\pi^0$, with $D^0 \rightarrow K^-\pi^+$ (a) for ΔE sidebands and (b) for ΔE consistent with zero. The curve in (a) is a fit to the background distribution described in the text, while in (b) the shape from (a) is used with the normalization allowed to float and a signal Gaussian of width 2.7 MeV is added.

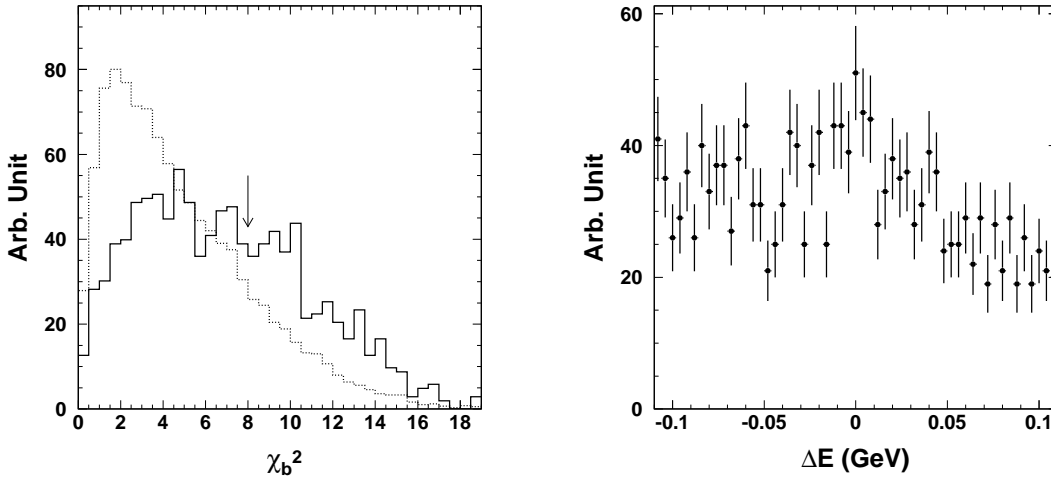


Figure 14: The χ_b^2 and ΔE spectra for the final state $D^{*0}\pi^+\pi^-\pi^-\pi^0$ with $D^0 \rightarrow K^-\pi^+$. For ΔE , the data are restricted to combinations within 2σ of the B^0 mass.

subsequently decays into $\pi^+\pi^-\pi^-$ and we produce a D^{*+} that decays into $D^{*+}\pi^0$. This process should be similar to that previously seen in the reaction $B^- \rightarrow D^{*0}\pi^-$, where the D^{*0} decayed into a $D^{*+}\pi^-$ [7]. We search for the presence of an a_1^- by examining the $\pi^+\pi^-\pi^-$ mass spectrum in Fig. 20. There is an excess of signal events above background in the a_1^- mass region, though it would be impossible to assert strong positive evidence. Proceeding by selecting events with $\pi^+\pi^-\pi^-$ masses between 0.6 and 1.6 GeV, we show the $D^{*+}\pi^0$ invariant mass spectrum in Fig. 21.

Although there is a suggestion of a low mass enhancement, it is not consistent with D^{**} production that would peak in region of 2.42 - 2.46 GeV. Perhaps we are seeing an indication of fragmentation at the $b \rightarrow c$ decay vertex here.

We also display for completeness the “ $a_1^-\pi^0$ ” mass distribution in Fig. 22. There may or may not be a wide structure in the $(4\pi)^-$ mass. At this point we abandon our search for substructure in this decay channel.

7 Discussion of Nature of the A^-

We speculate here on the nature of the A^- . Signals for $\omega^0\pi^-$ resonances have been detected before below 1500 MeV. There is a well established axial-vector state the $b_1(1235)$ with mass 1230 MeV and width 142 MeV. Data on vector states, excited ρ 's, is inconsistent. Clegg and Donnachie [8] have reviewed $\tau^- \rightarrow (4\pi)^-\bar{\nu}$, $e^+e^- \rightarrow \pi^+\pi^-$ and $e^+e^- \rightarrow \pi^+\pi^+\pi^-\pi^-$ data, including the $\omega\pi$ final state. Their best explanation is that of two 1^- states at 1463 ± 25 MeV and 1730 ± 30 MeV with widths 311 ± 62 and 400 ± 100 MeV, respectively. Only the lighter one decays into $\omega\pi$. The situation is quite complex, however. They conclude that these states must be mixed with non- $q\bar{q}$ states in order to explain their decays widths. There is also an observation of a wide, 300 MeV, $\omega\pi^0$ state in photoproduction at 1250 MeV [9], that apparently doesn't play a significant role in τ^- decays or e^+e^- annihilation. Our state is

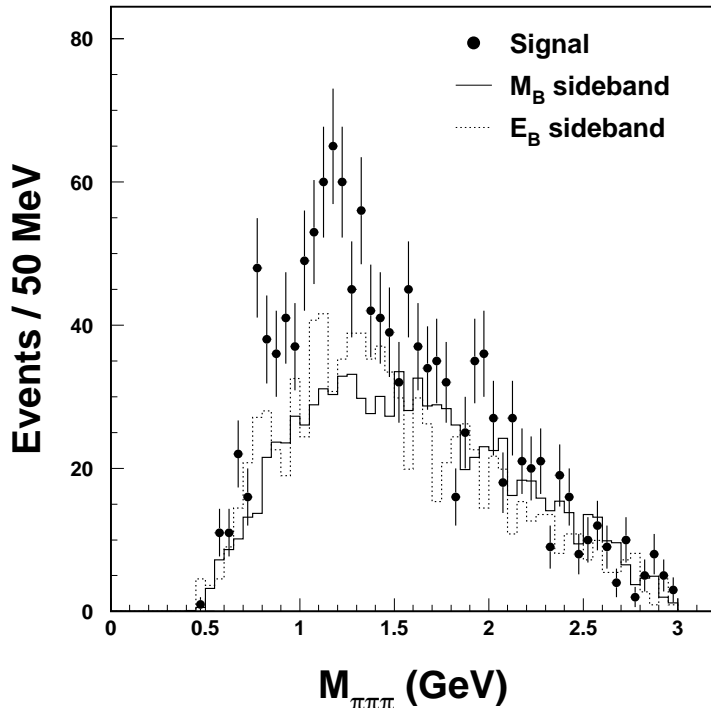


Figure 15: The invariant mass spectra of $\pi^+\pi^-\pi^0$ for the final state $D^{*0}\pi^+\pi^-\pi^-\pi^0$ for all three D^0 decay modes. The solid histogram is the background estimate from the M_B lower sideband and the dashed histogram is from the ΔE sidebands; both are normalized to the fitted number of background events. There are two combinations per event.

consistent with the lower mass ρ' . We do not seem to be seeing significant production of the higher mass state into $\omega\pi^-$, as expected. We limit

$$\frac{\Gamma(B \rightarrow D^*\rho'(1730))}{\Gamma(B \rightarrow D^*A^-(1436))} < 8.6\% \quad \text{at 90\% confidence level,} \quad (13)$$

using 400 MeV for the $\rho'(1730)$ width.

Several models predict the mass and decay widths of excited ρ and ω mesons [10]. For example, according to Godfrey and Isgur the first radial excitation of the ρ is at 1450 MeV. There is a large variation among the models, however, on prediction of the relative decay widths ranging from no $\pi\pi$ to $\pi\pi$ being equal to $\omega\pi$. One notes that previous CLEO data showed no $\pi^-\pi^0$ at the ρ' in $B \rightarrow D^*\pi^-\pi^0$ [4].

8 Conclusions

We have made the first statistically significant observations of four hadronic B decays: $\bar{B}^0 \rightarrow D^{*+}\pi^+\pi^-\pi^-\pi^0$, $\bar{B}^0 \rightarrow D^{*+}\omega\pi^-$, $B^- \rightarrow D^{*0}\pi^+\pi^-\pi^-\pi^0$ and $B^- \rightarrow D^{*0}\omega\pi^-$. The branching fractions have been measured.

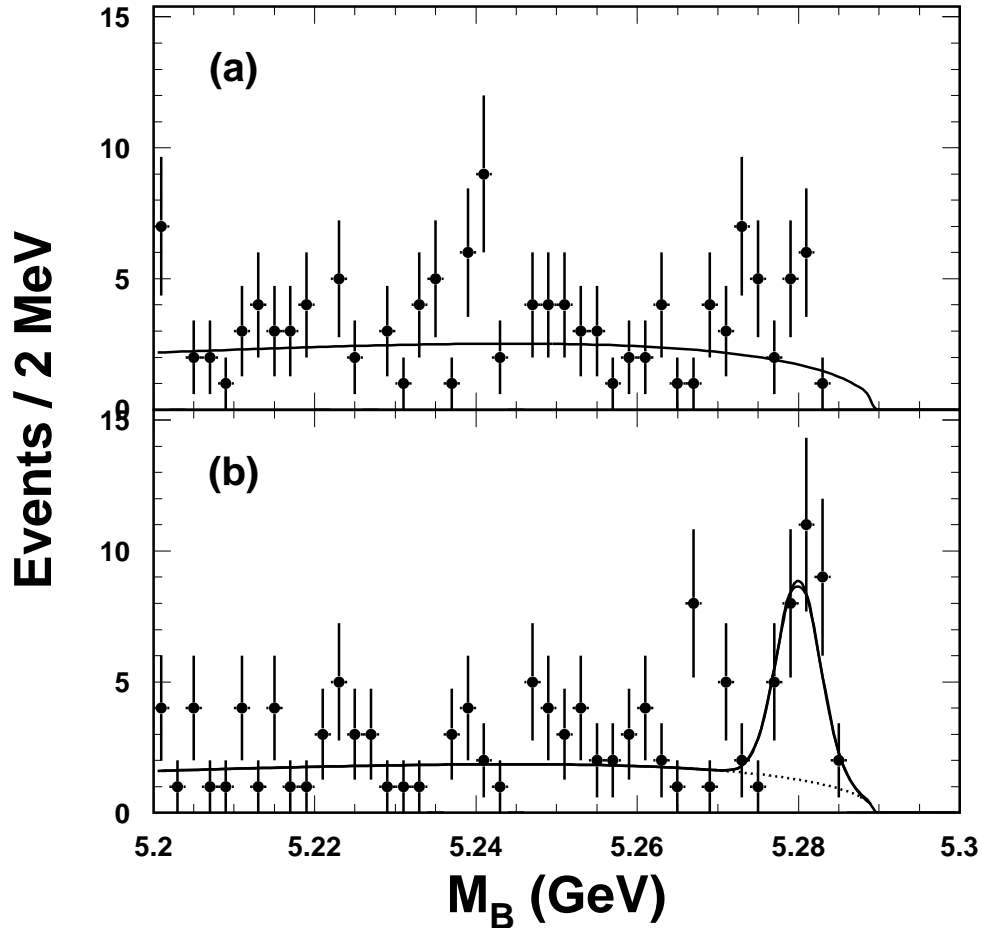


Figure 16: The M_B spectra for $D^{*0}\omega\pi^-$ for the $D^0 \rightarrow K^-\pi^+$ decay mode. (a) ΔE sidebands and (b) ΔE around zero.

There appears to be a resonant substructure in the $\omega\pi^-$ mass at 1419 ± 33 MeV with an intrinsic width of 382 ± 44 MeV. While it is possible that we are observing the ρ' final conclusions rest with more analysis including a determination of the spin and parity.

The final states with a D^* and $\pi^+\pi^-\pi^-\pi^0$ are quite complicated and are not dominated by only one decay mechanism.

We thank Marina Artuso for useful discussions about excited ρ 's.

References

- [1] C. Caso *et al.*, The European Physical Journal **C3** (1998) 1.

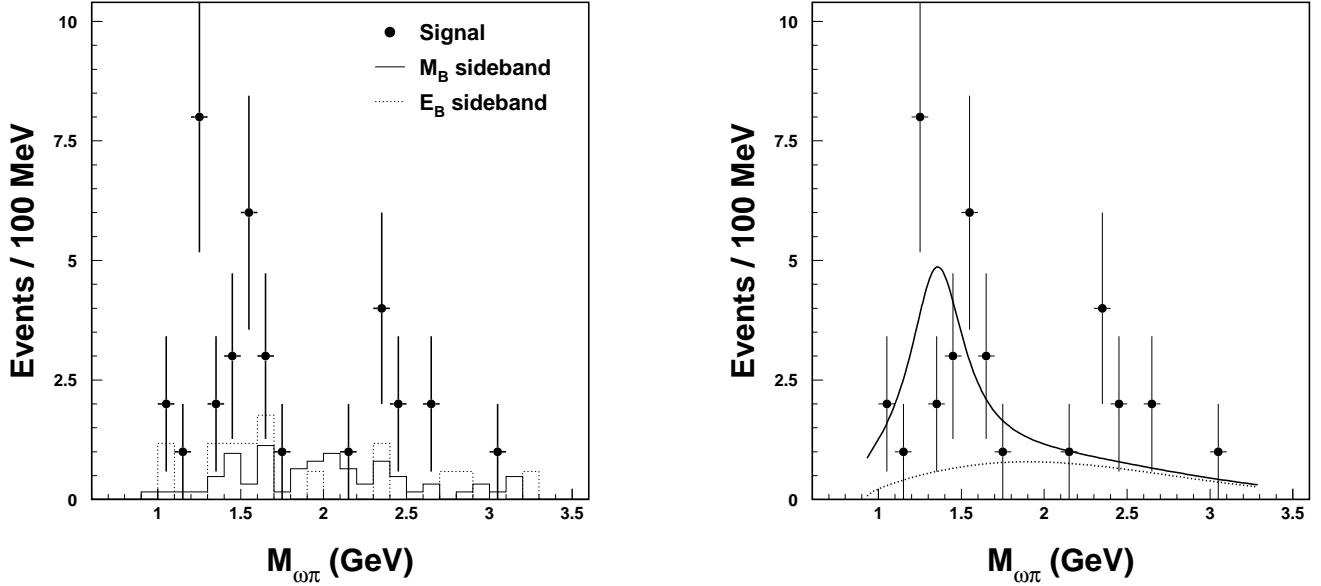


Figure 17: The invariant mass spectra of $\omega\pi^-$ for the final state $D^{*0}\pi^+\pi^-\pi^-\pi^0$ for the $D^0 \rightarrow K^-\pi^+$ decay mode. (left) The solid histogram is the background estimate from the M_B lower sideband and the dashed histogram is from the ΔE sidebands; both are normalized to the fitted number of background events. (right) The data fit to a Breit-Wigner signal and a smooth background function.

- [2] G. Brandenburg *et al.*, “Charged Track Multiplicity in b Meson Decays,” CLNS 99/1626, hep-ex/9907057 (1999).
- [3] ARGUS previously reported a signal of 28 ± 10 events in this mode, corresponding to a branching ratio of $(3.4 \pm 1.8)\%$. H. Albrecht *et al.*, Z. Phys. **C 48**, 543 (1990).
- [4] M. Alam *et al.*, Phys. Rev. **D 50**, 43 (1994).
- [5] G. Fox and S. Wolfram, Phys. Rev. Lett. **23**, 1581 (1978).
- [6] S. Schuh and S. Stone, CBX 00-7.
- [7] M. S. Alam *et al.*(CLEO), Phys. Rev. **50**, 43 (1994); S. Anderson *et al.*(CLEO), “Observation of a Broad $L = 1$ cq state in $B^- \rightarrow D^{*+}\pi^-\pi^-$ at CLEO,” CONF 99-6 (1999).
- [8] A. B. Clegg and A. Donnachie, Z. Phys. **C 62**, 455 (1994).
- [9] D. Aston *et al.*, Physics Lett. **92B**, 211 (1980).
- [10] S. Godfrey and N. Isgur, Phys. Rev. **D 32**, 189 (1995); G. Busetto and N. Oliver, Z. Phys. **C 20** 247 (1983); R. Kokoski and N. Isgur, Phys. Rev. **D 35** 907 (1987).

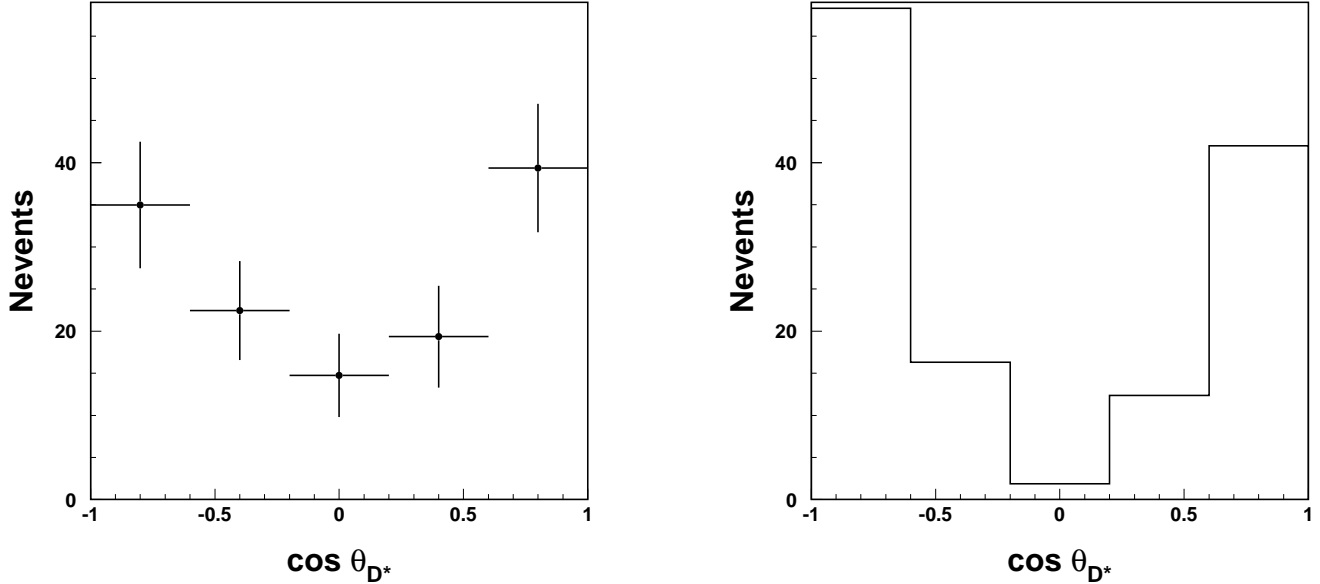


Figure 18: The cosine of the angle between the D^0 and the D^* flight direction in the D^* rest frame for the $D^* A^-$ final state. (left) Data in the M_B signal interval shown as points with error bars. (right) The Monte Carlo expectation including detector acceptance for a spin-0 A^- .

9 Appendix: Details of Selection Requirements

9.1 Charged Track Cuts

Tracks must pass Trackman.

Kin_{cd} must be zero.

These are the only cuts for the slow pion from the D^{*+}

For other tracks above 250 MeV we require $dbcd < 0.005$ and $|z0cd - zvptx| < 0.03$

If the track is below 250 MeV we require $dbcd < 0.01$ and $|z0cd - zvptx| < 0.05$

9.2 Particle Identification Cuts

For tracks above 900 MeV/c we do not require any particle identification.

For tracks below 900 MeV/c we require 3σ consistency, if the information is present ($iqaldi > 0$).

9.3 Photon Selection

We use XBAL.

We require that the bump energy be > 30 MeV in the good barrel region, $\cos \theta < 0.707$.

The E9/E25 distribution must look like a photon, $e925u > c92501$.

Photon candidates must not be shower fragments, $ibstop = 0$.

Finally, the angle with closest charged track must be $> 20^\circ$.

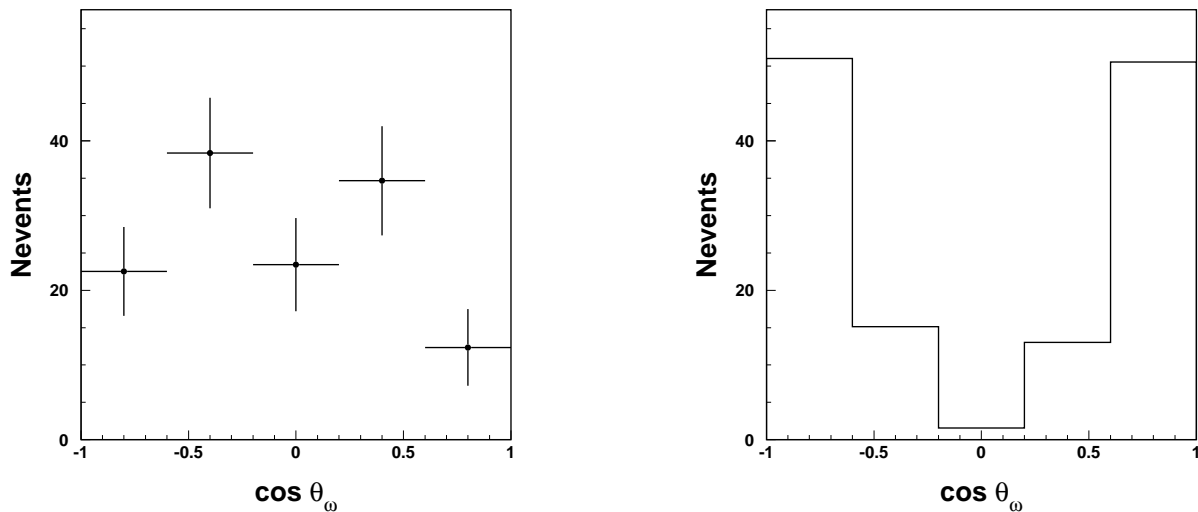


Figure 19: The cosine of the angle between the ω and the A^- flight direction in the A^- rest frame for the D^*A^- final state. (left) Data in the M_B signal interval shown as points with error bars. (right) The Monte Carlo expectation including detector acceptance for a spin-0 A^- .

9.4 π^0 Selection

If both bumps belong to a multi-bump region, they must come from the same region.

We require that the diphoton invariant mass be between -3.0 to $+2.5\sigma$, where $\sigma = 5.46$ MeV.

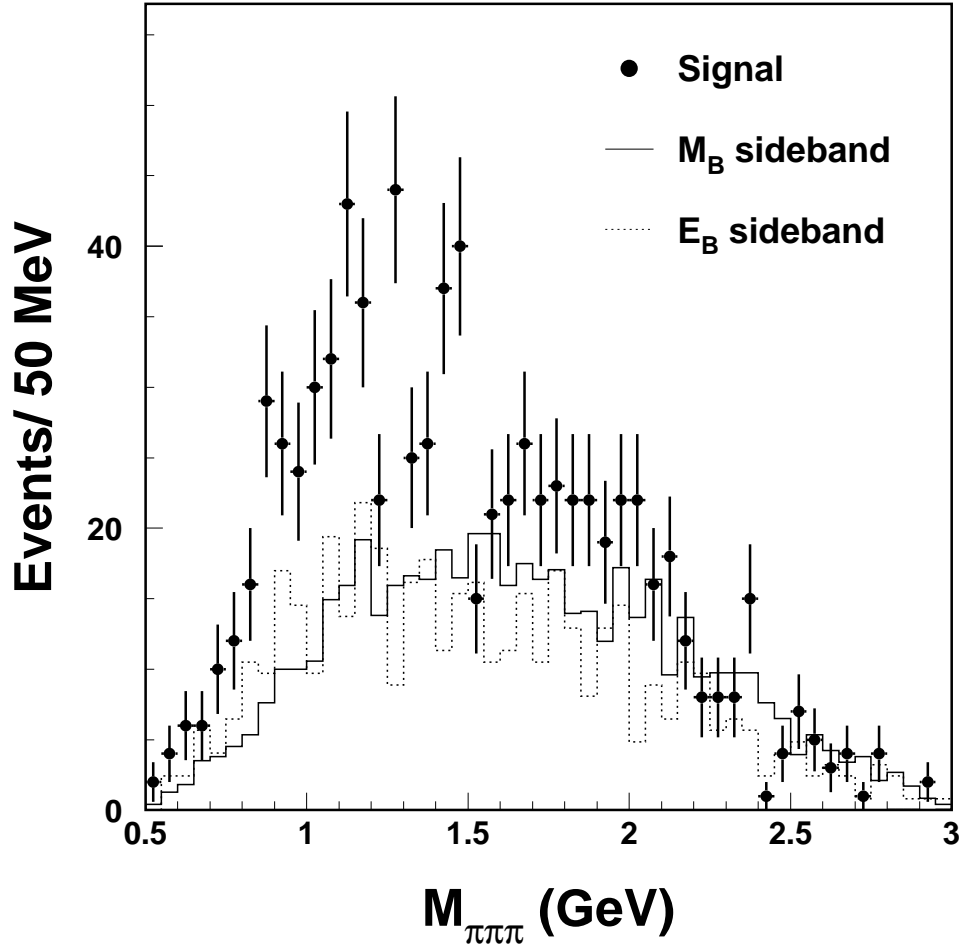


Figure 20: The invariant mass spectra of $\pi^+\pi^-\pi^-$ for the final state $D^{*+}\pi^+\pi^-\pi^-\pi^0$ for $D^0 \rightarrow K^-\pi^+$. The solid histogram is the background estimate from the M_B lower sideband and the dashed histogram is from the ΔE sidebands; both are normalized to the fitted number of background events.

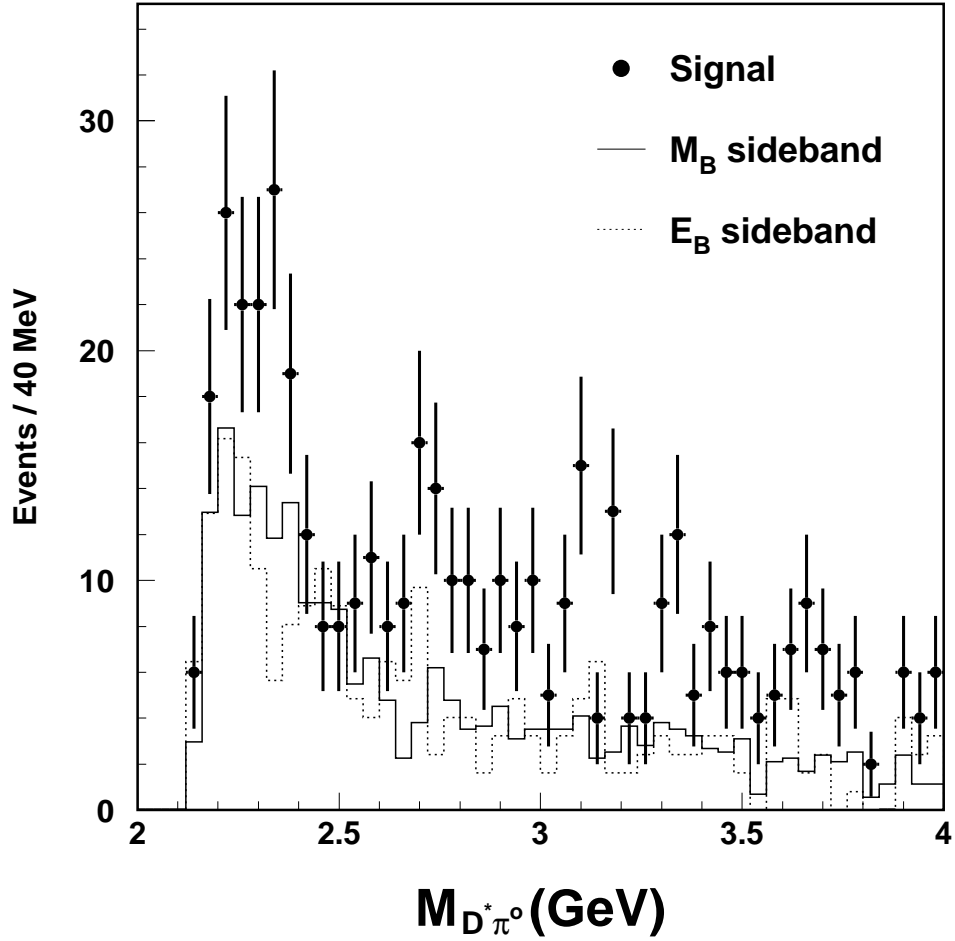


Figure 21: The invariant mass spectra of $D^{*+} \pi^0$ for $\pi^+ \pi^- \pi^- \pi^0$ masses between 0.6 - 1.6 GeV. for the final state $D^{*+} \pi^+ \pi^- \pi^- \pi^0$ with $D^0 \rightarrow K^- \pi^+$. The solid histogram is the background estimate from the M_B lower sideband and the dashed histogram is from the ΔE sidebands; both are normalized to the fitted number of background events.

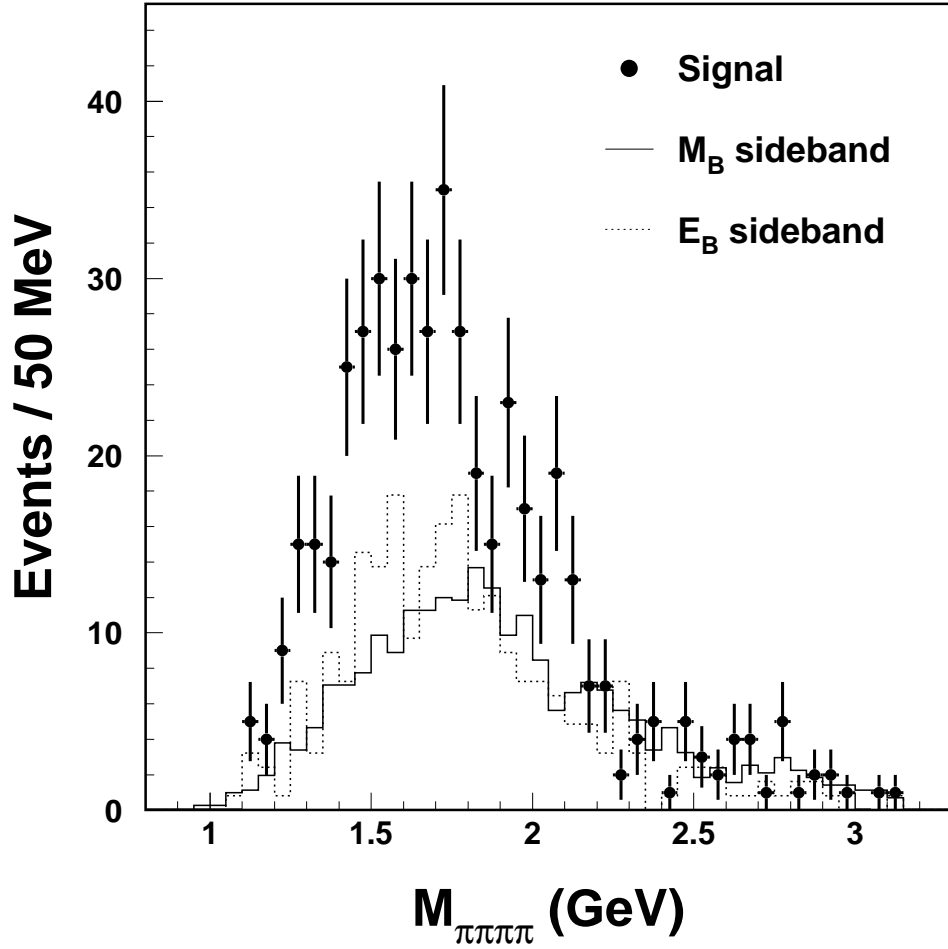


Figure 22: The invariant mass spectra of $\pi^+\pi^-\pi^-\pi^0$ for $\pi^+\pi^-\pi^-$ masses between 0.6 - 1.6 GeV, for the final state $D^{*+}\pi^+\pi^-\pi^-\pi^0$ with $D^0 \rightarrow K^-\pi^+$. The solid histogram is the background estimate from the M_B lower sideband and the dashed histogram is from the ΔE sidebands; both are normalized to the fitted number of background events.